Monthly Notices of the ROYAL ASTRONOMICAL SOCIETY

MNRAS **464,** 2866–2881 (2017) doi:10.1093/mnras/stw2641
Advance Access publication 2016 October 13

Numerical simulations of oscillation-driven regolith motion: Brazil-nut effect

Clara Maurel,[1]★ Ronald-Louis Ballouz,[2,3] Derek C. Richardson,[2] Patrick Michel[3] and Stephen R. Schwartz[3]

[1]*Institut Supérieur de l'Aéronautique et de l'Espace (ISAE-Supaéro), University of Toulouse, F-31055 Toulouse Cedex 4, France*
[2]*Department of Astronomy, University of Maryland, College Park, MD 20742, USA*
[3]*Lagrange Laboratory, University of Nice-Sophia Antipolis, CNRS, Observatoire de la Côte d'Azur, F-06300 Nice, France*

Accepted 2016 October 12. Received 2016 September 6; in original form 2016 September 6; Editorial Decision 2016 October 11

ABSTRACT

Many if not most small asteroids are rubble piles covered by regolith, and small perturbations may be enough to disturb their surfaces in complex ways due to microgravity. Experiments to study low-gravity regolith dynamics are challenging, and properly validated numerical simulations can provide valuable insights. In this paper, we investigate numerically size segregation among regolith grains, which is likely to occur after repeated shaking events. In particular, we are interested in the so-called Brazil-nut effect (BNE), i.e. the migration of a large intruder towards the top of a vertically shaken granular system. We go a step forward in simulating this effect by implementing horizontal periodic boundary conditions (PBC) in the *N*-body code PKDGRAV, with the aim of making the simulations more representative of the expected asteroid environment. We study the influence of PBC on the BNE in Earth gravity and compare them with a walled case. We also investigate the influence of static and rolling friction on the BNE. With walls, we observe the well-known convection mechanism driving the BNE. However, we find that a different mechanism, consisting of void filling, is responsible for the BNE with PBC, and we discuss its relevance in light of previous studies. By running simulations in $10^{-4}g$, we show that this void-filling mechanism remains relevant in a low-gravity environment. However, we find that depending on the gravity level, the void-filling mechanism is differently influenced by the friction properties of particles. We speculate that this is likely due to a change in the granular flow time-scales.

Key words: methods: numerical – comets: general – minor planets, asteroids: general.

1 INTRODUCTION

Asteroids, like planets, are driven by a great variety of both dynamical and physical mechanisms but in a much weaker gravitational environment. Given their wide range of sizes and surface compositions, it is clear that many asteroids and other small Solar system bodies formed in very different places and at different times within the solar nebula. Sizes, shapes, as well as rotational, internal and surface properties of asteroids are in fact the outcome of a collisional and dynamical evolution which has moulded them since their formation. Past encounters of probes with different asteroids completely renewed our vision of these objects from a geological point of view. This geological perspective now encompasses a wide range of processes including avalanches, impacts and seismic events, even if these processes are still not well understood for asteroid environments. The understanding of the processes experienced by asteroids, especially the way these processes change their physical properties and influence their evolution, serves as a tracer of the past and future story of the small-body population in the Solar system.

Particle segregation is one of the processes which seems to play a critical role in the evolution of asteroid surface properties, and possibly internal ones (Murdoch et al. 2015). Main Belt collisional evolution models suggest that a majority of asteroids of size ranging from a few hundreds of metres to about 50 km are of second generation at least, i.e. are born as a result of the collision between two parent bodies (Bottke et al. 2005, 2015). Numerical simulations of catastrophic disruption (Michel et al. 2001, 2015) indicate that those second-generation bodies are generally gravitational aggregates, formed by reaccumulation of ejected fragments, and thus can be modelled as granular systems (Richardson et al. 2002). Moreover, the vast majority of their surfaces seem to be covered in regolith, another kind of granular medium, as suggested by thermal inertia

★ E-mail: clara.maurel@isae.fr

measurements (Delbo' et al. 2007, 2015) and direct images (e.g. on Eros, Asphaug et al. 2001, and Itokawa, Miyamoto et al. 2007). The granular properties of regolith are still poorly understood, as well as the diversity of these properties among the asteroid population. For instance, the two near-Earth asteroids visited by spacecraft so far, i.e. the 17-km size Eros (NASA – *NEAR*-Shoemaker) and the 320-metre size Itokawa (JAXA – Hayabusa), possess thoroughly different regolith properties, despite their same S taxonomic type: a thick layer of fine grains was found on Eros, while a shallow layer of gravel-like grains was found on Itokawa (Yoshikawa et al. 2015). In addition to the asteroids' different dynamical and collisional histories, their different gravitational environments likely have a strong influence on the variety of their surface properties. However, both Eros and Itokawa show big boulders on their surfaces (e.g. Barnouin-Jha et al. 2008) surrounded by smaller grains. This characteristic is particularly striking on Itokawa, whose gravity is so less that the common invocation of gravitational capture of ejecta after impact cratering can hardly explain the presence of large rocks at the surface. In fact, ejection speeds of excavated material are expected to exceed the escape speed of the asteroid (a few tens of cm s^{-1}). Michel & Richardson (2013) proposed that the boulders at the surface of Itokawa result from the asteroid's formation process: after the disruption of its parent body, Itokawa could have formed by gravitational reaccumulation of ejected fragments.

However, regolith segregation and more specifically the Brazil-nut effect or BNE (Rosato et al. 1987) may be another process responsible for the presence of big boulders at the surface of asteroids. The BNE consists of large particles rising up through a granular medium composed of smaller grains, when the latter is repeatedly shaken. On an actual asteroid, the occurrence of this effect could be the result of seismic shaking induced by thermal cracking (Delbo et al. 2014) or multiple micro-impacts experienced by the asteroid over its lifetime (e.g. Cheng et al. 2002; Richardson, Melosh & Greenberg 2004). Seismic shaking and the resulting motion of regolith material were invoked to explain the paucity of small craters on Eros and Itokawa (Richardson et al. 2004; Michel et al. 2009) as well as the formation of ponds on Eros (Cheng et al. 2002). In addition, they may also cause particle segregation. This could explain the presence of big boulders at the surface, and also imply that an asteroid's interior could be composed of smaller particles than those observed at the surface, suggesting a variation of macroporosity with depth. Therefore, particle segregation and BNE might have important implications in the arrangement of asteroid surfaces and interiors.

Two issues arise with the BNE. First, the mechanism driving the BNE is still not fully established and doubts remain about its unicity (Kudrolli 2004). In particular, granular convection is a process often invoked as the origin of granular segregation at the surface of asteroids (Asphaug 2007; Miyamoto et al. 2007). However, granular convection is strongly dependent on the gravitational acceleration and it has been shown that a weak gravitational acceleration may reduce the efficiency of particle size segregation (Gray & Thornton 2005; Murdoch et al. 2013). Moreover, recent numerical simulations and parabolic flight experiments show that the rising speed of a large intruder through a granular material decreases with the external gravity (Tancredi et al. 2012; Güttler et al. 2013; Matsumura et al. 2014). Therefore, asteroids with their low gravity should not be the most suitable place for such a process. However, as the typical lifetime of asteroids of similar or larger size than Itokawa is greater than tens of millions of years (e.g. Bottke et al. 2005), provided that the meteoroid flux is efficient enough to induce repeated shaking events, particle segregation may have time to occur despite the low-gravity conditions. The second issue is that the BNE is known to occur in a confined, walled environment (such as the one used by e.g. Tancredi et al. 2012 and Matsumura et al. 2014), which does not seem to be the best representation of an asteroid interior or near-surface. A numerical study by Perera et al. (2016) showed that a rubble-pile asteroid, made up of a population of particles of two different sizes, will show size segregation for sufficiently high impact energies. Their study showed that size segregation can occur on a global scale without the need of a confining wall; however, their simulations were limited to showing segregation of large 40-m and 80-m size particles. Thus, although these experimental and numerical studies greatly helped to improve our understanding of the size segregation process and its sensitivity to various parameters (e.g. gravity, friction coefficients), the conclusions need to be confirmed in an environment more consistent with the one expected on an actual asteroid surface.

The aim of this paper is to accomplish a step towards this goal by numerically investigating the BNE in an unconfined environment, using periodic boundary conditions (PBC). Particle size segregation is, in this case, not influenced by the confinement caused by walls of the container and the potential occurrence of the BNE will therefore only be due to the interaction among particles. If BNE occurs under such conditions, the possibility of an extrapolation to the asteroid environment will be strengthened. We investigate the differences in behaviour of the large intruder when wall boundaries are either present or absent, and also specifically focus on the influence of the static and rolling friction properties of the grains. We also get closer to realistic asteroid environments by performing the same simulations in low gravity, such as those encountered on Itokawa-like asteroids. Understanding how a granular medium with a size distribution may segregate in an unconfined environment can allow us to better assess the porosity and grain distribution on asteroids.

Today, we only have direct access to global bulk densities through space missions (e.g. Yeomans, Konopliv & Barriot 1997; Fujiwara et al. 2006), study of the Yarkovsky effect (Chesley et al. 2003) or binary asteroid observations (Merline & Chapman 2001). This new aspect of investigation may be of great value for indirectly estimating the density heterogeneity within asteroids. Considering the paucity of direct measurements, the community needs other means to derive information from indirect measurements, through e.g. the modelling of different dynamical processes possibly contributing to the evolution of the asteroids' internal structure. This paper offers a contribution to this effort. In Section 2, we provide details on the *N*-body code PKDGRAV used in this study, along with the various parameters investigated, with and without PBC. Results are presented and analysed in Section 3, and are followed by complementary analysis, interpretation and discussion in Section 4. Conclusions and proposed future work are found in Section 5.

2 METHODOLOGY

2.1 Numerical tool: PKDGRAV

All the simulations presented in this paper were performed with the parallel *N*-body gravity tree code PKDGRAV (Stadel 2001), adapted to model collisions between solid spherical grains by Richardson et al. (2000, 2009, 2011). PKDGRAV uses a second-order leapfrog integrator, computing at each time-step accelerations due to gravity and contact forces. A soft-sphere discrete element method (SSDEM) has been implemented to treat collisions between particles, accounting for the various kinds of friction experienced at contact (Schwartz, Richardson & Michel 2012). In particular, in order to simulate the

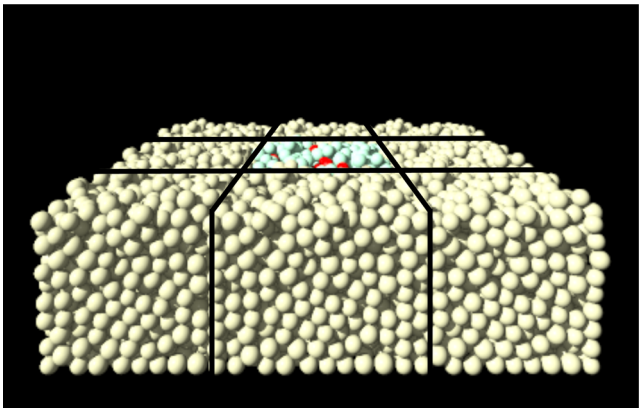

Figure 1. Initial setup for a periodic boundary simulation. Central pattern is surrounded by eight replicas made of ghost particles. Lines were added to help visualize the replicated patterns. The colours of the real particles are varied for better visualization.

microdeformations which occur when two grains collide (or when a grain collides with a boundary such as a wall), they are allowed to overlap slightly, generally by no more than 1 per cent of the radius of the smallest particle. Note that PKDGRAV looks for every overlap between particles at each time-step and warns the user if these overlaps exceed the desired threshold. SSDEM is described in detail in Schwartz et al. (2012). Therefore, in the following, we only make a brief review of the overall method, and establish the terminology used in this paper.

When two particles overlap, they both experience a repulsive spring force, whose normal and tangential components are characterized by the spring constants k_n and k_t. The kinetic friction is represented by the normal and tangential damping of the spring, with damping coefficients C_n and C_t. However, in this study, we use the more familiar normal and tangential coefficients of restitution ϵ_n and ϵ_t, obtained as a combination of C_n, C_t, k_n and k_t (see Schwartz et al. 2012). Conventionally, we adopt $k_t = (2/7)k_n$. Static friction at the contact point generates a tangential force, parametrized by the static-limit coefficient μ_s. Our implementation also provides rolling friction parametrized by the coefficient μ_r. In the following, we assume zero twisting friction ($\mu_t = 0$), which means that the spin around a contact point is not damped. This assumption is commonly made when an ensemble of grains is considered.

In our study, we make use of PBC. Doing so, we can study particle segregation for an ensemble of particles which are freely vibrating without a surrounding physical boundary. PBC are imposed on a patch of particles by replicating the patch in the horizontal directions (x–y), perpendicular to the oscillating direction (z). Each replicated patch contains ghost particles which match the relative positions of the original particles. Particles near the boundary edges may interact in collision with ghost particles. Fig. 1 illustrates an initial setup with PBC.

2.2 Friction parameters

One aspect of this study is to analyse how material properties influence the outcomes of the simulations. Given the strong uncertainties concerning the granular properties of asteroids, we performed simulations using a broad spectrum of friction coefficients. Each grain in the system was simulated with the same set of coefficients. We made the choice to focus on materials of medium-to-high levels of static and rolling friction, starting in the range where the BNE is

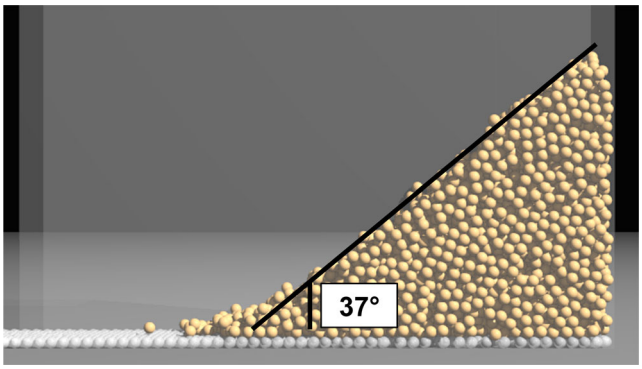

Figure 2. High-friction 'gravel' material system at equilibrium after the release of the grains. Here the final achieved angle of repose is 37° (see Table 1).

expected to occur with wall boundaries under Earth gravity, and pushing to levels where friction might impede this effect.

Matsumura et al. (2014) studied the influence of friction on the rise of the 'Brazil nut' for static and rolling friction parameters, respectively, μ_s and μ_r, between 0.0 and 0.9, using PKDGRAV and cylindrical containers. Their results showed that certain values of friction parameters were more favourable to the BNE: $\mu_s \gtrsim 0.5$ and $\mu_r \lesssim 0.2$. They obtained these thresholds with coefficients of restitution $\epsilon_n = 0.5$, $\epsilon_t = 0.5$ and for an amplitude and frequency of oscillation $A = 1$ cm and $\omega = 93.9$ rad s^{-1}, respectively. We based the lower limit of the investigated range of friction on a set of parameters identified by Matsumura et al. (2014) as leading to the rise of a big intruder in an oscillating bed of small grains: $\mu_s = 0.8$, $\mu_r = 0.2$ and medium dissipation of the grains with $\epsilon_n = 0.5$, $\epsilon_t = 0.5$. Note that this set may not necessarily reflect properties of a material existing on Earth. As an upper limit, we defined a gravel-like material (Yu et al. 2014), characterized by $\mu_s = 1.3$, $\mu_r = 2.0$, and again $\epsilon_n = 0.5$, $\epsilon_t = 0.5$. This very high friction aims to represent the behaviour of irregularly shaped grains which resist flow even though we are using spherical particles. If we were able to simulate true angular shapes, these coefficients would likely be smaller compared to their current values. We also implemented a 'control' material, for which we did not expect to see the intruder rise. For this, we used a set of parameters mimicking the behaviour of glass beads, a low-friction material ($\mu_s = 0.43$, $\mu_r = 0.1$) with a very small amount of dissipation ($\epsilon_n = 0.95$, $\epsilon_t = 1.0$). This set of material parameters was calibrated against avalanche experiments by Richardson et al. (2012).

These three sets of material parameters were compared to the literature by carrying out angle-of-repose simulations. Grains of 0.5-cm radius were initially contained, at equilibrium, in a rectangular box. Then, by removing one side of the box, they were allowed to fall through an extended container, paved with a layer of similar grains glued to the floor (to create a rough surface). We recorded the evolution of the slope formed by the pile of particles and calculated the resulting slope angle, which converged to the value of the angle of repose once the equilibrium state was reached. Fig. 2 shows the equilibrium state for the gravel-like material and the corresponding angle of repose. The values of the angles of repose for the different materials are summarized in Table 1. The angles obtained belong to the ranges which can be found in the literature: $\phi(^\circ) \in [21,25]$ for glass beads (e.g. Barabási et al. 1999) and $\phi(^\circ) \in [32,40]$ for gravel-like material (e.g. Orlova 1962).

We performed a series of simulations for equally distributed values of friction parameters ranging between moderate and the

Table 1. Coefficients of restitution and friction of the simulated glass beads, and of the materials representing the lower and upper limits of the range of static and rolling friction investigated. These are compared to the ranges found in the literature.

Parameters	Glass beads	Moderate friction	Gravel-like
ϵ_n	0.95	0.5	0.5
ϵ_t	1.0	0.5	0.5
μ_s	0.41	0.8	1.3
μ_r	0.1	0.2	2.0
ϕ (°)	19.5	27.5	37.0
Barabási et al. (1999)	[21,25]	–	–
Orlova (1962)	–	–	[32,40]

gravel-like values: $\mu_s \in [0.8, 1.3]$ in steps of 0.1 and $\mu_r \in [0.2, 2.0]$ in steps of 0.2, with $\epsilon_n = 0.5$, $\epsilon_t = 0.5$ throughout. Each of these simulations was repeated 10 times (3 times for the cases in a low-gravity environment – see Section 3 for details), with walls and PBC, each time starting with a new random initialization to ensure the independence of the simulations. In summary, we had a total of 60 simulations repeated 10 (or 3) times, for both walls and PBC cases, in addition to the control simulation with glass beads.

Note – The rolling friction model used for this study is the same as that in Yu et al. (2014) and Matsumura et al. (2014). The latest version of PKDGRAV has an optional new rolling friction model which uses a rolling force spring (Zhang et al. 2016). This new model is particularly important to treat quasi-static problems. In our case, however, the BNE simulations are strongly dynamic and the conclusions should not suffer from a change in the rolling friction model. We tested this by conducting a limited number of runs comparing intruder rise speeds for the two models, using roughly equivalent material parameters and found no substantial differences. We refrain from using this model for the majority of our simulations as it adds to the computational cost of a simulation.

2.3 PKDGRAV parameters and walls setup

In our simulations, two key parameters are the normal spring constant k_n (see Section 2.1) and the simulation time-step δt. The value of k_n was chosen so that the maximum overlap of particles was no more than 1 per cent of the smallest particle radius for the entire simulation. The time-step was then chosen so that collisional loading and unloading of the spring takes at least 30 steps. This means that the time-step is always very small compared to the gravitational dynamical time of the system. In this simulations, the acceleration of the bottom wall is several times the local gravity, and constrains the required time-step and normal spring constant necessary to properly resolve particle–particle and particle–wall collisions. The values of k_n and δt are given by

$$k_n \approx m \left(\frac{v_{max}}{x_{max}}\right)^2 \quad ; \quad \delta t \approx \left(\frac{m}{k_n}\right)^{1/2}, \tag{1}$$

where m is the typical mass of the particles, v_{max} is the maximum expected particle speed and x_{max} is the maximum overlap when two particles collide, 1 per cent of the smallest particle radius in this case (see Schwartz et al. 2012). When maximum particle speeds in the simulations are sufficiently below the sound speeds of the simulated material, and when perturbations propagate through the domain faster than the dynamical times relevant to the simulated regime, matching the material sound speed is not required to produce meaningful results. In our simulations, the maximum expected particle speeds are less than a third of the sound speed of the material. Therefore, we use a 1 per cent maximum overlap criterion to resolve collisions in the subsonic regime in a computationally efficient manner.

The small bed particles in our simulations are spheres with a normal distribution of radii of mean $r_p = 0.5$ cm, with a standard deviation 0.05 cm, and a cutoff at ± 1 standard deviation. The Brazil nut has a radius of $r_{BN} = 1.5$ cm. These values were chosen for their convenience regarding computational time. Although BNE may involve metre-size boulders on actual asteroids, we expect the effect to scale to larger size, up to the limit where self-gravity becomes non-negligible. The density is $\rho_P = 2700$ kg m^{-3} for each particle, meaning the large intruder is 27 times more massive than a small particle in the granular bed. In order to estimate k_n and δt, we used the mean bed-particle mass as the typical value for m and their mean size to evaluate x_{max}. Also, v_{max} is the speed of the oscillating wall (i.e. $v_{max} = A\omega = 93.9$ cm s^{-1}; see below). From this, we derived the following values for k_n and δt:

$$k_n \approx 5 \times 10^5 \text{ kg s}^{-2} \quad ; \quad \delta t \approx 4 \times 10^{-6} \text{ s}. \tag{2}$$

With PKDGRAV, particles are allowed to interact with each other as well as with walls. One of our main objectives is to compare walls cases and PBC cases. In order to make walls and PBC setups as similar as possible, every wall uses the same coefficients of restitution and friction as the grains. In every walls case, lateral walls form a parallelepiped open on the top of a 10×10 cm base, which is high enough to prevent any escape of the particles once oscillations of the bottom plate start. The choice of a rectangular container is different from the one of Matsumura et al. (2014), who performed all their simulations with a cylindrical container. However, as PBC require rectangular boundaries, the walls cases have to be performed with a rectangular container to ensure a relevant comparison. In order to evaluate the influence of the container's geometry, we carried out pairs of simulations aiming to compare, under different conditions of friction, the outcomes of a simulation inside a cylinder and inside a parallelepiped. We found that in all cases, both geometries led to the same result (either no rise of the Brazil nut at all or full rise) within a comparable amount of time. Consequently, we assumed that for our purposes, the use of a parallelepiped container had no significant influence on the outcomes of the simulations compared to the use of a cylinder.

Finally, we set the oscillation of the bottom wall (and lateral walls if they exist) to a frequency $\omega = 93.9$ rad s^{-1} and an amplitude $A = 1$ cm. These values match the fiducial choice of Matsumura et al. (2014) and represent a dimensionless acceleration of $\Gamma = \frac{A\omega^2}{a_g} \approx 9$ for simulations under Earth gravity (a_g is the gravitational acceleration taken equal to $1g$). This value of Γ will be kept the same throughout the study, even for simulations under low gravity, as another means of ensuring the validity of our comparisons.

2.4 Initialization process and main simulations

The initialization process was the same for the walls and PBC simulations. In order to avoid any bias due to a uniform placement of the grains, we generated randomly the particles inside an ellipsoidal volume large enough to avoid contacts between the grains. This volume was suspended above the parallelepiped container and particles were allowed to fall inside the container under Earth gravity. The Brazil nut was positioned a few millimetres above the floor of the container and small grains fell from a few tens of centimetres. This way, the large intruder was at the bottom of the system at the end of the filling phase. Once the particles were at equilibrium inside the

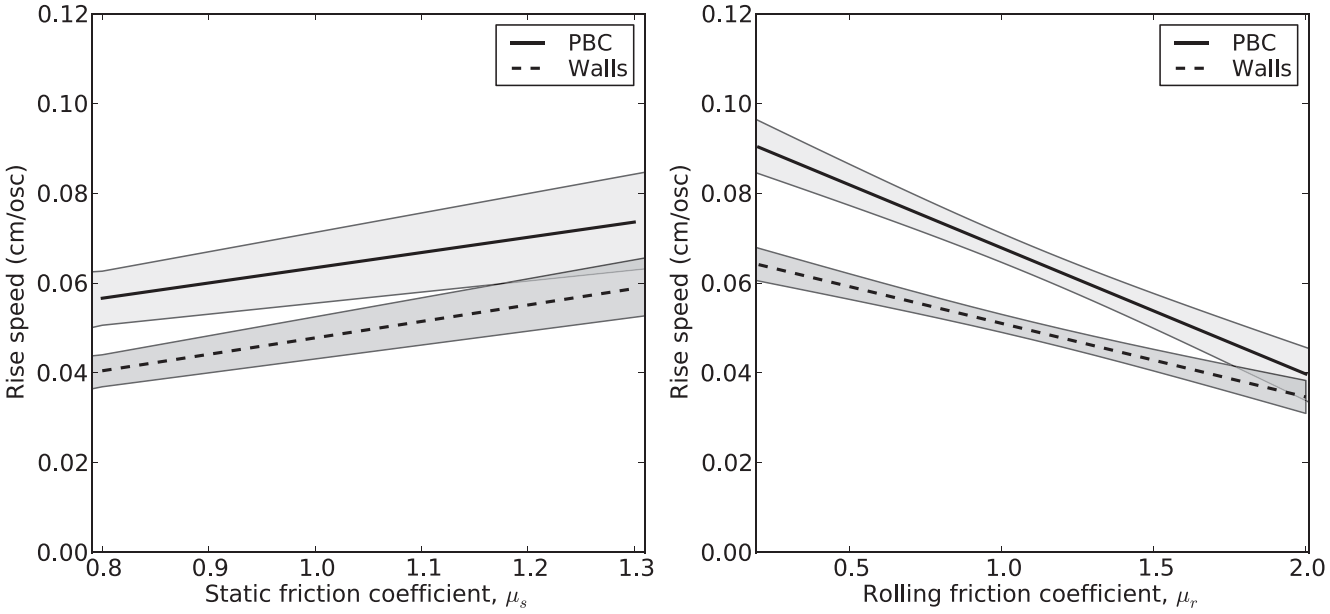

Figure 3. Least-squares regression lines showing the evolution of the mean rise speed of the Brazil nut with μ_s (left) and μ_r (right), for walls cases (dashed line) and PBC cases (solid line). The lines are obtained by fitting the data of the series of 10 simulations, all values of μ_r and μ_s mixed up, respectively, for the left- and right-hand panels. Shaded areas show the 95 per cent confidence intervals for the fits.

container, we could either start walls cases or turn on the PBC and remove the lateral walls. The central patch of particles, in the latter case, was thus surrounded by a layer of replicas. The particles were then allowed to re-equilibrate before starting the main simulations.

As mentioned in Section 2.3, we gave the bed particles a small size distribution. This prevented artificial packing of the particles while filling the container or during a main simulation. Fill-ups were performed separately for each configuration of (μ_s, μ_r).

3 RESULTS

In this section, we present the results of the various simulations described in the previous section. We first report on the results obtained under Earth gravity, by analysing the differences in outcomes between PBC and walls cases, emphasizing on the influence on the BNE of static and rolling friction levels. In the second part, we present the results obtained in a low-gravity environment. Further analysis and discussions about the results are found in Section 4.

3.1 Earth-gravity cases: walls versus PBC

The principal observation which can be made while running identical simulations performed with walls and PBC in Earth gravity is that final outcomes of both configurations are relatively similar. If the Brazil nut rises up with a walls case, it also rises in the associated PBC case, but if it does not rise in certain conditions, it will not rise with PBC either. For example, as already shown by Matsumura et al. (2014) with walls, the simulation involving glass beads resulted in no net ascension of the intruder, independent of the boundary conditions. Conversely, with grains of moderate friction ($\mu_s = 0.8$ and $\mu_r = 0.2$), the BNE occurred with walls as well as with PBC. Therefore, we confirm here that BNE does not necessarily require a confined environment to occur. However, although the system achieves a similar final state in both cases, the mechanism driving the BNE is different. Here, we present the relevant results, which are analysed and contextualized in Section 4. As a means of comparison, we focus in this section on the rise speed of the Brazil nut. Doing so, we can include in the analysis the cases where the intruder starts rising but does not reach the top within the time of the simulation (arbitrarily fixed). The rise speed is measured in centimetres per oscillation (cm/osc). Recall from Section 2.2 that, to provide better statistics, we performed 10 times independently the 60 simulations derived from the chosen range of μ_s values (from 0.8 to 1.3) and μ_r values (from 0.2 to 2.0), each time with an independent initialization. Thus, for each value of μ_s, we had $10 \times 10 = 100$ cases (one for each value of μ_r, for 10 simulations), and $10 \times 6 = 60$ cases for each value of μ_r. In total, we had 600 simulations for both walls and PBC configurations.

In this section, we are interested in comparing the global behaviour of the walls cases to that of the PBC cases. To do so, we focus on the evolution of the rise speed with μ_s for all values of μ_r mixed up (i.e. independent of μ_r), and similarly, the evolution of the rise speed with μ_r, for all the values of μ_s mixed up. The question of the influence of μ_r for a given μ_s and vice versa will be addressed in Section 3.2. Fig. 3 shows the least-squares regression lines obtained by fitting the 600 values of rise speed as a function of μ_s (left-hand panel) and μ_r (right-hand panel), for PBC and walls cases. For reasons of clarity, the 1200 individual scatter points are not plotted, but shaded areas show the 95 per cent confidence intervals for the fits.

At first glance, the left-hand panel of Fig. 3 suggests that, in both walls and PBC cases, the higher the value of μ_s, the higher the mean rise speed of the Brazil nut. In addition, this growing trend is similar in both cases. In the right-hand panel of Fig. 3, the opposite trend appears. The mean rise speed of the intruder decreases with an increasing value of the rolling friction coefficient μ_r. This time, a steeper slope is evident for PBC cases, meaning that with PBC, the rise of the intruder is more affected by the level of rolling friction than with walls. Finally, looking at both panels, the mean rise speed of the Brazil nut with PBC seems to be globally higher than that with walls. This last observation would suggest that either the same mechanism is driving the BNE in both cases, but it is more efficient with PBC, or two different mechanisms are actually

Table 2. Values of the test statistic obtained from equation (3). From left to right, the two first columns correspond to walls cases, and the other to PBC cases. The left column of each set of two (labelled 'RS $= f(\mu_s)$') gives the t-value corresponding to the slope of the regression line shown in the left-hand panel of Fig. 3. This t-value shows how significantly the walls and PBC cases are affected by an increase of the static friction level. The right column (labelled 'RS $= f(\mu_r)$') gives the t-value corresponding to the lines in the right-hand panel of Fig. 3, which characterize this time the effect of rolling friction level on the walls and PBC cases. The critical t-value for 95 per cent confidence, t_{crit}, is given at the top of the table. The t-values are underlined if they are above t_{crit}.

$t_{crit} = 1.96$				
	Walls cases		PBC cases	
	RS $= f(\mu_s)$	RS $= f(\mu_r)$	RS $= f(\mu_s)$	RS $= f(\mu_r)$
t-value	6.04	9.39	3.34	9.92

leading the BNE with walls and PBC. The difference in steepness of the slopes in the right-hand panel of Fig. 3 would actually support the second hypothesis. However, before elaborating on this, we performed a series of statistical tests on the raw data to strengthen our forthcoming conclusions. For this, we used a variation of the Student t-test adapted to the study of the slope of regression lines. The objective was threefold: (1) ensure that the trends visible on Fig. 3 are not artefacts due to a linear regression made on dispersed data; (2) check whether the two slopes in the left-hand panel of Fig. 3 are statistically equal and whether the two slopes of the right-hand panel are significantly different; and (3) assess whether the intercepts of the PBC and walls lines are statistically different from each other. We will first present the three tests and their results successively, before elaborating on the actual information we can get from these results.

Test (1) requires comparing the four slopes of linear regression in Fig. 3 to zero. If the corresponding test statistics are higher than a critical value, the null hypothesis is rejected, and the slopes would indeed have a significant steepness. To compare a slope to zero, the following test statistic can be used:

$$t = \frac{|\, b \,|}{s_b}, \tag{3}$$

where b is the slope of the regression line considered, and s_b is a function of the standard deviation of the abscissa values (μ_s or μ_r) and of the standard error of the estimate, which measures the accuracy of predictions made by the regression line. This t-value is then compared to a critical value t_{crit} found on Student's law table, which depends on the number of available data and on the desired confidence interval. Here, for 600×2 available data and a 95 per cent confidence interval, Student's law table gives $t_{crit} \sim 1.96$. The four calculated values of t are summarized in Table 2 (two for the evolution of the mean rise speed in walls and PBC cases with μ_s, and the two others with μ_r). Each t-value of Table 2 being greater than t_{crit}, this test ensures that statistically, the mean rise speed of the Brazil nut is indeed affected by an increasing level of static and rolling friction, whether walls or PBC are turned on. However, Test (1) does not compare walls and PBC cases to each other.

Test (2) requires comparing the slopes of the PBC and walls regression lines to each other. The test statistic which can be used is given by

$$t = \frac{|\, b_w - b_{pbc} \,|}{\sqrt{s_{b_w}^2 + s_{b_{pbc}}^2}}. \tag{4}$$

Table 3. Values of the test statistic obtained from equation (4). These values show how significantly the evolution of the mean rise speed with respect to μ_s (left column) and μ_r (right column) differs from PBC to walls cases. The critical t-value for 95 per cent confidence, t_{crit}, is given at the top of the table. The t-values are underlined if they are above t_{crit}.

$t_{crit} = 1.96$		
	RS $= f(\mu_s)$	RS $= f(\mu_r)$
t-value	0.17	3.52

Table 4. For each panel of Fig. 3 ('RS $= f(\mu_s)$' and 'RS $= f(\mu_r)$') is given the confidence interval for the value of the intercept of the line corresponding to the walls-cases regression line subtracted from the PBC-cases regression line. The value zero belonging to both intervals, we cannot conclude that the intercepts of the walls and PBC cases are significantly different.

$t_{crit} = 1.96$		
	RS $= f(\mu_s)$	RS $= f(\mu_r)$
Confidence interval	$[-0.05\,;0.02]$	$[-0.05\,;0.002]$

Here, $b_{w/pbc}$ is the slope of the corresponding regression line (walls or PBC), and $s_{b_{w/pbc}}$ is the corresponding value of s_b. The critical value remains $t_{crit} \sim 1.96$, and Table 3 shows the two t-values which compare the evolution of mean rise speed with μ_s (left) and μ_r (right) between walls and PBC cases. As expected from Fig. 3, this test ensures that statistically the mean rise speed of the Brazil nut is similarly affected by the level of static friction (the slopes are statistically equal), whether walls or PBC are turned on ($t_{\mu_s} < t_{crit}$). On the other hand, the effect of μ_r on the mean rise speed of PBC cases is significantly different for walls and PBC cases.

To complete the set of statistical verifications, we want to assess whether the intercepts of the regression lines in each case (left- and right-hand panels of Fig. 3) are significantly different. For this, we subtract one regression line from the other and find the confidence interval of the resulting predicted value when $x = 0$ (y-intercept). If 0 belongs to the confidence interval, it means that the intercept of the line resulting from the subtraction can be zero, and therefore that the two intercepts cannot be significantly distinguished. Table 4 shows the confidence intervals for each panel of Fig. 3. Here, the visual interpretation was actually misleading, and we cannot say that the mean rise speeds of PBC cases are statistically higher than that of walls cases.

To summarize, Fig. 3 visually suggests that BNE could, under Earth gravity, be driven by a different mechanism with PBC compared to with walls. Our results suggest that whatever the mechanism is which drives the BNE for PBC, it has a similar dependence on the static friction as the mechanism driving the BNE with walls. However, the BNE mechanism involved in PBC has a stronger dependence on the rolling friction than the BNE mechanism involved with walls. The previous statistical tests, however, help us to qualify these first conclusions. So far, we know that, for both PBC and walls cases, the mechanism driving the BNE is sensitive to the level of static friction (the mean rise speed increases with μ_s) and the level of rolling friction (the mean rise speed decreases with μ_r). Moreover, with PBC, the influence of μ_r is significantly more important than with walls, whereas the influence of μ_s is at first glance similar. Finally, we cannot conclude from the present analysis that the BNE mechanism with PBC is making the intruder rise faster than with

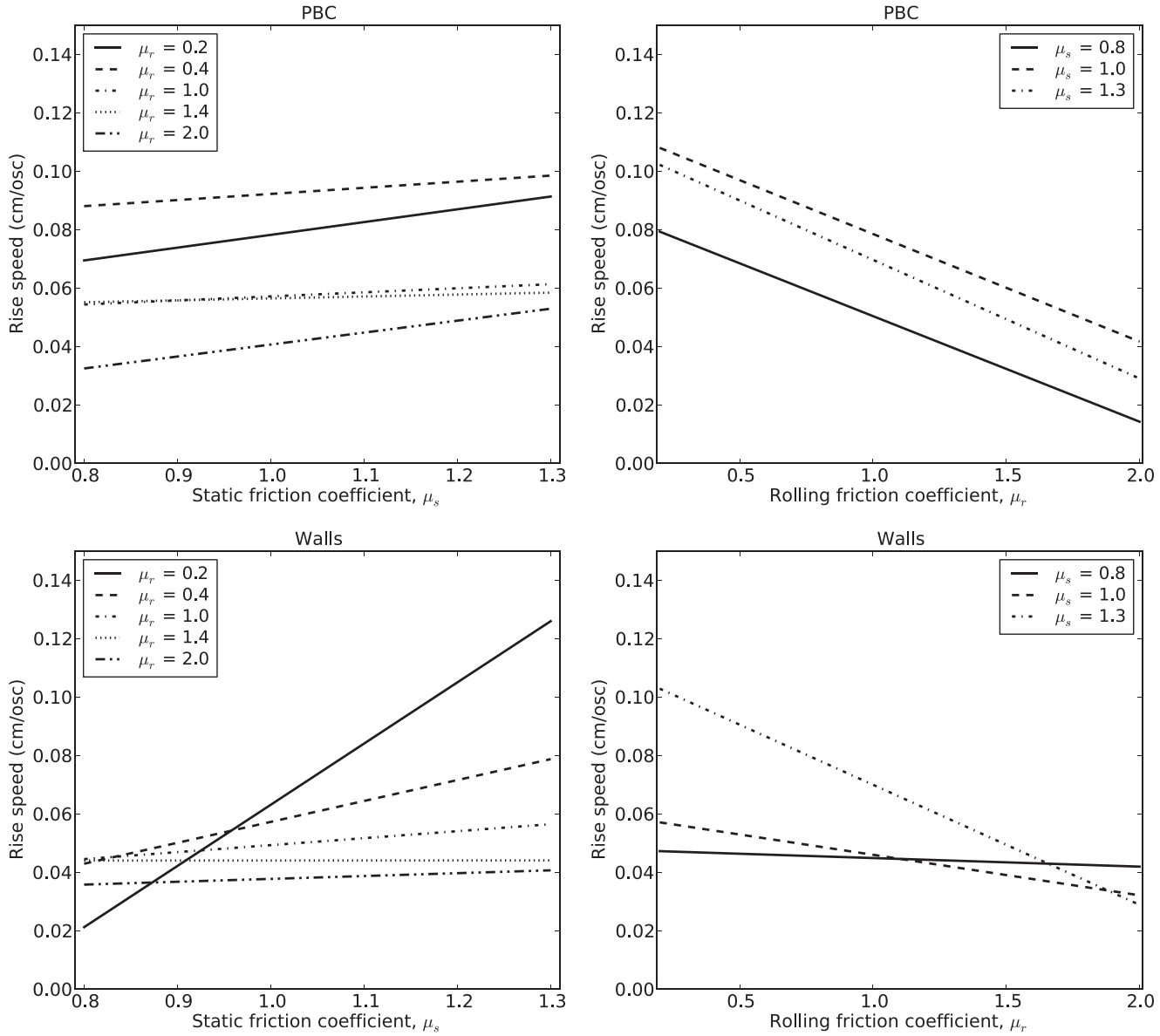

Figure 4. Regression lines obtained by fitting the data of the series of 10 simulations for PBC cases (top) and walls cases (bottom). The left-hand panels represent the evolution of the rise speed with μ_s for different values of μ_r, while the right-hand panels show the evolution with μ_r for different values of μ_s.

walls, as the intercept of the regression lines on Fig. 3 are actually not significantly different.

At this point, further analysis is needed to discriminate the mechanisms driving BNE with PBC and walls, provided that they are different. For this, we no longer focus on the mean rise speed, but on the influence of the static and rolling friction at given values of μ_r and μ_s, respectively.

3.2 Earth-gravity cases: specific influence of static and rolling friction levels

Fig. 4 shows the regression lines obtained by fitting the data of the series of 10 simulations for PBC cases (top) and walls cases (bottom). However, unlike Fig. 3 where all values of friction parameters are mixed up, each line represents a certain level of rolling friction (left-hand panels) and static friction (right-hand panels). For clarity, the 95 per cent confidence intervals are omitted from these plots. For PBC cases, these intervals are globally ±0.02 cm/osc for the top-left panel and ±0.01 cm/osc for the top-right panel. For walls cases, in the bottom-left panel, we find a maximum of ±0.04 cm/osc for the confidence interval of the $\mu_r = 0.2$ fitted line, while for all other lines we find ±0.01 cm/osc. In the bottom-right panel, we also find a larger confidence interval for the $\mu_s = 1.3$ curve (±0.02 cm/osc), and ±0.01 cm/osc otherwise. Interestingly, Fig. 4 seems to imply an important difference in behaviour of the Brazil nut between walls and PBC cases. Even in the worst-case scenarios, the larger intervals found for Walls cases do not change the visible trends.

Let us first focus on walls cases (bottom panels). In the left-hand panel, we see that the lower the value of μ_r, the more important the influence of μ_s on the rise speed of the intruder. For example, for $\mu_r = 0.2$ (solid line), the least-squares linear regression shows that the rise speed can increase from approximately 0.02 cm/osc at $\mu_s = 0.8$ to more than 0.12 cm/osc at $\mu_s = 1.3$, while for $\mu_r = 2.0$ (double-dot–dashed line), the influence of μ_s on the rise speed

seems to be insignificant. Moreover, this trend is strongly correlated with the values of μ_r. The influence of μ_s decreases rapidly with increasing μ_r, and then stagnates at almost zero. A clear trend is also visible in the bottom-right panel of Fig. 4. At low levels of static friction, the influence of μ_r on the rise speed is hardly visible (solid line); however, at high μ_s (dash–dotted line), the rise speed can decrease by approximately a factor of 10 between $\mu_r = 0.2$ and $\mu_r = 2.0$, again with a correlation between the values of μ_s and the importance of its influence on the rise speed. These observations were validated by the same statistical test as Test (2), in which we compared the slopes two by two. The results of this test were in agreement with the trend visible in Fig. 4.

On the other hand, the influence of static and rolling friction levels in PBC cases is not so clearly brought out by the top panels of Fig. 4. Neither the influence of μ_s on the rise speed of the intruder nor the influence of μ_r seems to be correlated with an increase or decrease of μ_r and μ_s, respectively. In fact, the slope of each regression line in the left- and right-hand panels looks relatively similar. This was confirmed by performing Test (2) again: no clear trend and no significant difference between a majority of slopes was found. In addition, the values of the intercepts of the regression lines are also not clearly correlated with an increase of μ_r or μ_s. Fig. 4 might suggest the existence of an efficiency threshold for values of μ_r and μ_s, respectively, around 0.4 and 1.0 (which give the highest intercept), but more data would be required to confirm or refute this hypothesis.

In light of the above-mentioned results, we claim that a different mechanism is driving the BNE with walls compared to with PBC. In fact, with walls, the efficiency of the process (characterized here by the rise speed of the Brazil nut) is highly dependent on the values of μ_r and μ_s: at low rolling friction levels, the process is catalysed by an increasing level of static friction. However, a higher level of rolling friction completely inhibits this effect. In contrast, at low levels of static friction, the influence of μ_r on the rising process is almost non-existent, whereas for a higher μ_s, an increase of the rolling friction level impacts drastically and negatively the rise speed of the intruder. It is well known that, under certain conditions (level of friction, frequency and amplitude of the oscillations), friction between particles and walls engenders a convective motion (e.g. Knight, Jaeger & Nagel 1993), with particles rising through the centre of the container and sinking along the walls. The results presented above seem to adequately characterize such a mechanism. The convective motion needs a certain level of static friction between the walls and the small grains to take place. As this level gets higher, the convection rolls form more and more easily (very likely until a certain limit, apparently not reached in our simulations). However, all this depends on the level of rolling friction. If particles are hardly able to roll on each other, the whole inward stream (inside the layer of particles which are in contact with the walls) is inhibited and the intruder rises more slowly.

With PBC, the very different behaviour of the Brazil nut for the same static and rolling friction conditions strongly suggests that BNE is driven by a mechanism different from convection. This mechanism is marginally affected by the level of static friction but is, however, more dependent on the level of rolling friction. In addition, the top panels of Fig. 4 show a more stochastic behaviour of the rise speed than for walls cases, for which the correlation between rise speed, μ_s and μ_r is demonstrated. To further strengthen the suspicion that convection is not the leading mechanism for BNE when PBC are turned on, we analysed the flow of particles for several simulations, with walls and PBC, as illustrated in

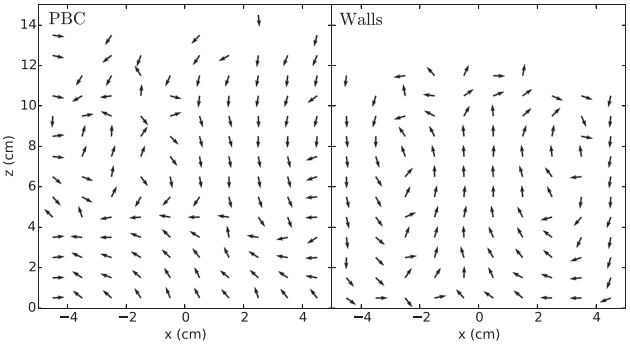

Figure 5. By tracking the change in particle positions over a single forcing period, we can visualize the convective motion of grains in simulations with wall boundaries (right) and the lack of convective motion in simulations with periodic boundaries (left). Both of these cases are for grains with friction parameters $\mu_s = 0.9$ and $\mu_r = 1.4$ (relatively high friction).

Fig. 5. This figure was created by considering a five-particle-wide cross-section of the centre of the container (the selection was done along the y-direction). A grid consisting of cells which are one particle wide is superimposed on the x–z plane. For every cell, the average displacement of particles from that cell to adjacent cells is tracked and plotted. In order to properly visualize the flow of particles, it is necessary to isolate the relative displacement of a particle with respect to other particles from the overall shaking motion of the entire medium. This is accomplished by only considering particle positions at the same phase of an oscillation cycle. We chose the zero phase of the oscillation, where the bottom plate has zero displacement and is moving in the positive z-direction. Fig. 5 shows a snapshot of this average motion of particles. The right-hand panel, representing a walls case, clearly shows a convective motion of particles, as a thin particle-wide layer is forced downwards along the walls. This forces the centre of the bed and the Brazil nut to move upwards. This pattern of granular convection is apparent throughout all walls simulations. The left-hand panel does not show a similar convective motion for the PBC cases. Rather, we find that most PBC cases show more-randomized and less-uniform motion. There are some cases where the convective pattern visible in the right-hand panel is seen intermittently in PBC cases; however, it only lasts for a few forcing cycles before it disappears. Hence, due to the absence of boundaries, convection cycles do not appear strongly when PBC are turned on, and despite that, we do see the Brazil nut rising. A further analysis of the leading mechanism for BNE in the absence of confining walls is proposed in Section 4.

3.3 Low-gravity cases

Our final objective was to see how our findings might extend to a realistic asteroid gravity environment. For this, we performed a suite of simulations with a local gravity set to 10^{-4} times Earth gravity ($10^{-4}g$), which is equivalent to the surface gravity on an Itokawa-sized body (Michikami et al. 2008). We re-initialized the grains in the low-gravity environment and allowed them to settle as explained in Section 2.4. This was again done for walls and PBC cases. To accurately compare these low-gravity simulations to those done in $1g$, we modified the shaking frequency of the granular bed such that Γ remains the same ($\Gamma \approx 9$; see the end of Section 2.3). As a consequence, we first adopted a shaking frequency of 0.939 rad s^{-1}, while keeping the amplitude of the oscillation at 1 cm. This allowed us to use a time-step of $\delta t \approx 3.7 \times 10^{-4}$ s for these

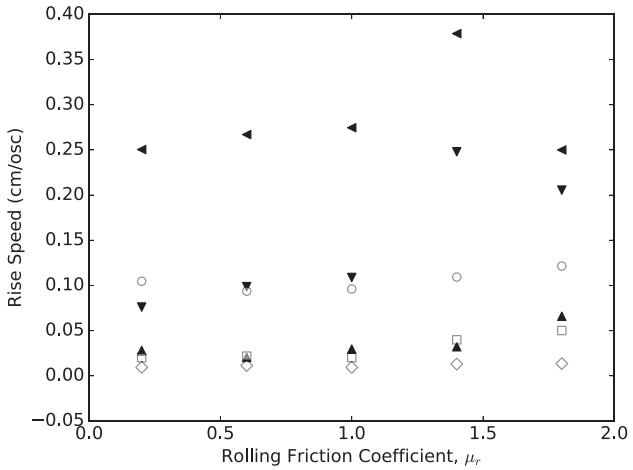

Figure 6. Rise speeds of the Brazil nut for simulations with a local gravity of $10^{-2}g$. The open symbols represent simulations where the particle collisions are resolved with spring constants similar to those in the $1g$ simulations, with $\mu_s = 0.8$, 1.0, and 1.2 represented by diamonds, squares, and circles, respectively. The spring constants and the time-step used in these simulations are very conservative values. The filled triangles represent simulations where the spring constants are chosen based on maintaining a maximum possible fractional overlap of 1 per cent, with $\mu_s = 0.8$, 1.0, and 1.2 represented by up-, down-, and left-facing filled triangles, respectively. The time-step varies by one order of magnitude between these two cases (with the filled symbols having a greater time-step).

low-gravity simulations. We maintained a maximum possible fractional overlap of ∼1 per cent by adjusting the value of k_n to $\approx 42\,\mathrm{kg\,s^{-2}}$. The value of k_t was then $\frac{2}{7}k_n \approx 12\ \mathrm{kg\ s^{-2}}$. This adjustment in the values of the spring constants is done for the sake of computational efficiency. If we were to maintain the same value of k_n as that used in the Earth-gravity simulations, the total time taken to complete each of the low-gravity simulations would increase by two orders of magnitude.

In order to ensure that this change in the value of k_n does not have a considerable impact on the outcome of our simulations, we ran a suite of simulations in a local gravity of $10^{-2}g$, where the value of Γ is again kept constant. Half of the simulations were done with a k_n and k_t, which is the same as that used in the $1g$ cases, and the other half were done with a k_n and k_t chosen to maintain a maximum possible overlap of 1 per cent (based on a vibrating bed with an oscillation frequency of 9.39 rad $\mathrm{s^{-1}}$ and an oscillation amplitude of 1 cm). The local gravity of $10^{-2}g$ was chosen with consideration for time constraints, since the slower simulations (those with spring constants similar to the $1g$ cases) were only one order of magnitude slower than simulations with spring constants chosen to maintain 1 per cent overlaps. We performed simulations with wall boundaries and chose three different values of μ_s (0.8, 1.0, 1.2) and five different values of μ_r (0.2, 0.6, 1.0, 1.4, 1.8). This small suite of simulations allows us to efficiently determine the magnitude of the influence of k_n in the rest of our simulations. The results of this test are shown in Fig. 6. Here, we show the variation in the time taken for the intruder to rise to the top of the granular bed. We find that for a wide range in μ_r, the rise speeds for various μ_s have similar magnitudes and variances for the two spring constant cases. For both cases, we find that the 'Brazil' nut rises with fairly similar speeds, the cases with a smaller k_n and larger time-step (filled triangles) bracketing the cases with a larger k_n and smaller time-step (open symbols). We conclude that, while there is some possible effect in the change of the particle spring constants, this effect is quite small. Furthermore, we find that both cases lead to similar trends across friction parameters, e.g. under $10^{-2}\ g$, the rise-speed increases as μ_s increases, independently of μ_r. Therefore, using a spring constant that allows for a faster computational time, while maintaining a small maximum fractional overlap, is acceptable for the current simulation setup.

For the cases with a local gravity $10^{-4}g$, the range of considered friction levels was similar to that described in Section 2.2: μ_s ranged from 0.8 to 1.3, and μ_r from 0.2 to 2.0. Again, we attempted to minimize any stochasticity that might arise from sample preparation by performing three separate simulations (with separate initializations) for each μ_s and μ_r pair. In total, we performed 360 simulations in the low-gravity regime (3 initializations, 2 boundary conditions and 60 unique friction pairs).

Overall, for a shaking amplitude of 1 cm and both PBC and walls scenarios, we were still able to observe the BNE occurring in almost all the simulations. Every walls case showed the intruder rising to the top of the granular bed in the time of the simulation, whereas for PBC simulations, it occurred in approximately 84 per cent of the cases (152 out of 180). The PBC cases which did not lead to a complete rise tended to be cases with low values of the rolling friction parameters ($\mu_r < 0.6$). In addition, these low-friction cases which did not result in a BNE tended to have the intruder begin to rise, but eventually stall at a system height lower than the barycentre of the system. These cases were omitted from subsequent analysis of rise speeds. Fig. 7 shows the average rise speeds for PBC (top panels) and walls (bottom panels) cases as a function of μ_s (left-hand panels) and μ_r (right-hand panels). The curves represent linear fits of three independent simulations (three different initializations of the granular bed). Like previous studies (Tancredi et al. 2012; Güttler et al. 2013; Matsumura et al. 2014), we find that, at moderate friction values, the rise speeds in a lower gravity environment are comparable to those under Earth gravity. Here, we also show that this result still holds even when PBC are used. However, unlike these previous studies, we have performed an exploration of the friction parameter (a proxy for material property) phase space in low gravity. This has resulted in some surprising outcomes.

For the PBC cases, we find that the magnitude of rise speeds in $10^{-4}g$ are similar to the $1\,g$ cases. Furthermore, similar to Earth gravity, we find that both the walls and PBC cases show a positive correlation with μ_s (see the left-hand panels of Fig. 7). However, the walls cases seem to have a stronger correlation with μ_s than the PBC cases. This likely points to a difference in the mechanism driving the BNE in each case, which is discussed further in Section 4. Furthermore, contrary to the Earth-gravity cases, we find that the rise speed in both PBC and walls cases is positively correlated with rolling friction, μ_r (compare the right-hand panels of Fig. 4 to Fig. 7). This positive correlation appears to be stronger for the PBC cases than the walls cases. For these PBC cases, we speculate that, in a low-gravity environment, the grains are lofted over a much longer period than under Earth gravity. This larger lofting period may give the grains more time to reconfigure, allowing for the entire system to re-settle with more voids (i.e. a smaller filling factor), as particles with a larger rolling friction can more easily maintain larger void spaces (in the other extreme, frictionless particles are more easily compacted into tighter spaces). As we will discuss in Section 4, larger void spaces in a granular system are important for the BNE to occur in a PBC system.

Previous studies (e.g. Matsumura et al. 2014) showed that the rise speed is generally constant across gravitational regimes (when scaling for the number of oscillations). In an absolute sense,

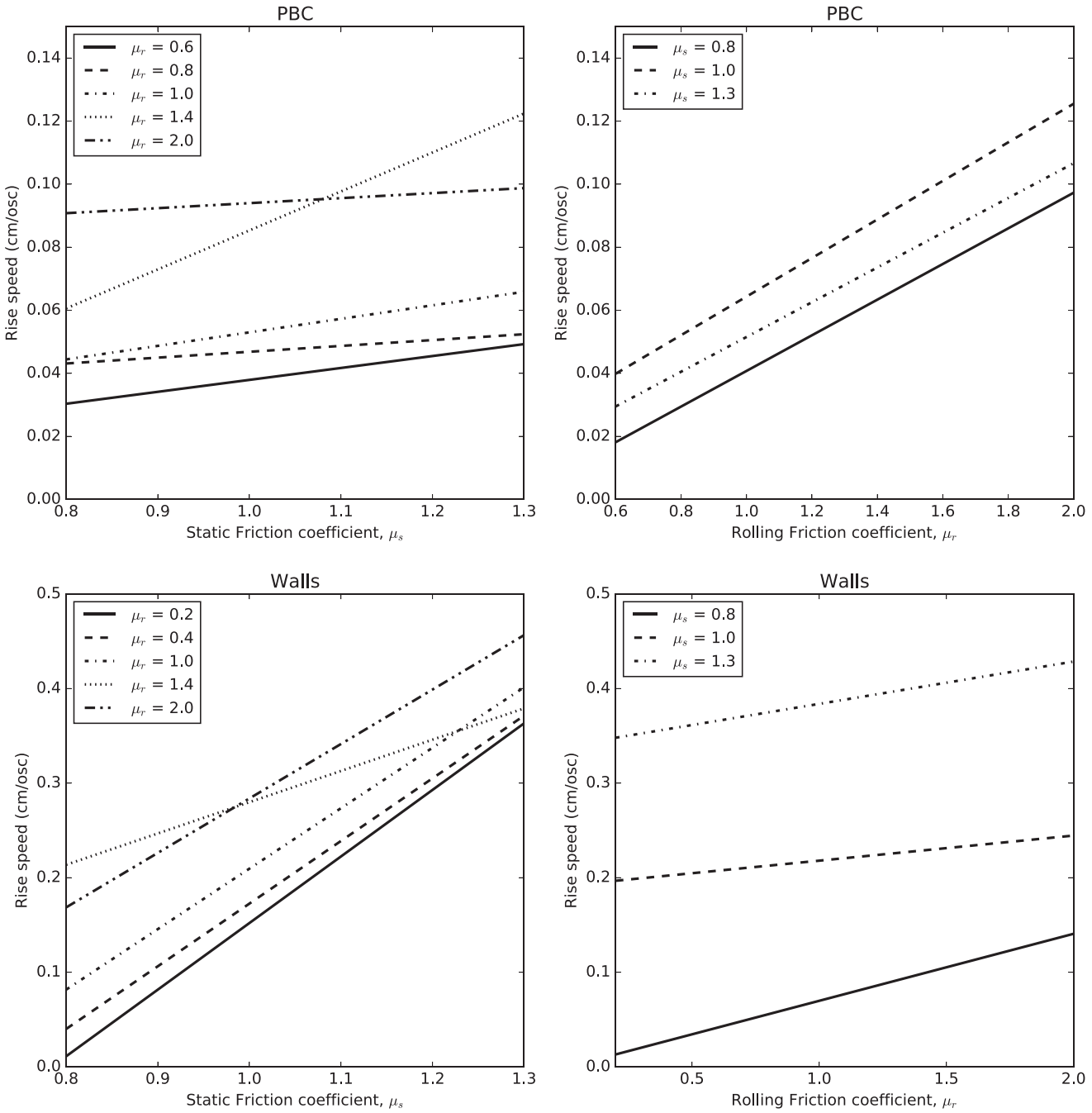

Figure 7. Rise speeds of the Brazil nut for simulations with a local gravity of $10^{-4}g$. The panels show lines which represent the linear trend of the rise speed with μ_s for different values of μ_r (left) and vice versa (right) with data extracted from three independent suites of simulations. The top panels show the results for cases with PBC, while the bottom panels show the results for walls cases.

Matsumura et al. (2014) showed that for a constant Γ, the rise speed of a system scales with the square root of the gravity of the system. In this study, we find that for low friction values, the magnitude of the rise speeds is consistent with this result, and that across four orders of magnitude in gravity, a variation of exactly two orders of magnitude in the oscillation frequency results in rise speeds which are within an order of magnitude of each other (in terms of cm/osc). Moreover, again at low friction values, comparable to those used in Matsumura et al. (2014), the rise speeds for the walls cases are very similar to that found in their $10^{-4}g$ case. However, this picture becomes challenged when varying the friction parameters towards higher values.

In $1g$ walls cases, we found that increasing μ_s from 0.8 to 1.3 leads to a factor of $\sim$6 increase in the rise speed (for low μ_r). In the $10^{-4}g$ cases, a comparable variation in μ_s leads to an increase in the rise speed by a factor of $\sim$20. For highly frictional particles, the efficiency of granular convection engendered by the presence of walls is enhanced in low gravity. We speculate that this may be due to differences in the packing of the granular bed (see Section 2.4) in low gravity. With a smaller overburden pressure on the grains at

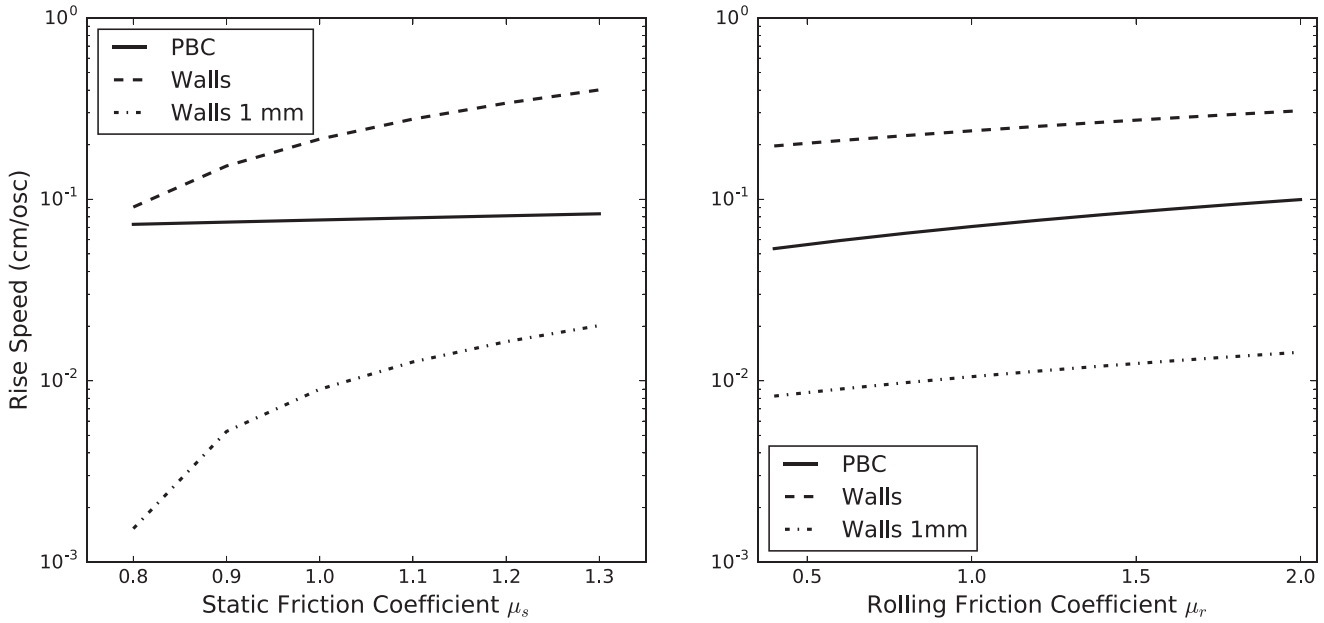

Figure 8. Average rise speeds of the Brazil nut for all simulations with a local gravity of $10^{-4}g$. The left- and right-hand panels show the rise speed as a function of μ_s and μ_r, respectively. Mean rise speeds are shown for simulations with an oscillation amplitude of 1 cm with PBC (solid line) and walls (dashed line). Oscillation amplitudes of 1 mm are also shown for walls cases (dot–dashed).

the bottom of the bed due to gravity, the upward ratcheting effect of granular convection may proceed much faster. While we can only speculate on an enhancement mechanism at this point, it is interesting to note that the data clearly show that the behaviour of the grains differs in a low-gravity environment. By varying the material properties of the grain, we can begin to probe the limits of possible behaviour of a granular system in microgravity.

To further mimic an actual asteroid environment, we deemed it necessary to test the effect of varying the frequency and amplitude of the oscillation to levels which might correspond to seismic shaking on a real asteroid. Several authors (e.g. Cheng et al. 2002 and references therein) claim that the seismic shaking which occurs on an asteroid may have frequencies of the order of a few hertz for millimetre-size amplitudes. In our case, the amplitude of the oscillation is 1 cm, which may still be an upper limit corresponding to more extreme shaking situations, but may not be representative of the vibrations induced by micrometeorite impacts. Garcia, Murdoch & Mimoun (2015) even find seismic wave amplitudes of the order of a few microns. Taking this information into account, we tested the effect of a smaller amplitude (always keeping the same value of Γ) and ran simulations with an amplitude of 1 mm and an oscillation frequency of 2.96 rad s^{-1}. This was done for a unique initialization of the granular bed. The 1 mm value was preferred to a smaller one, because a lower amplitude would have certainly resulted in poor results, as it would have represented less than 1/10th of a grain diameter.

Our initial expectation was that none or very few of the low-amplitude cases would actually exhibit the BNE, as previous studies (Matsumura et al. 2014) underlined the sensitivity of the BNE to the amplitude and frequency of the oscillation. According to their study, even amplitudes of half the grain size could lead to the disappearance of the BNE, even at high oscillation frequencies. For these smaller amplitude cases, approximately 60 per cent of the walls cases resulted in a full rise of the intruder, while only 6 per cent resulted in a BNE for PBC. Both boundary conditions showed a strong dependence of BNE occurrence on friction properties. For the Wall cases, only cases with $\mu_s > 0.9$ exhibited the BNE. For PBC, the few cases (5 in total) which did exhibit that BNE had high static and rolling friction ($\mu_s > 1.0$ and $\mu_r > 1.6$). In Fig. 8, we show the average rise speeds as a function of μ_s (left) and μ_r (right), for the three different types of simulation in $10^{-4}g$: PBC cases with 1-cm amplitude (solid line), walls cases with 1-cm amplitude (dashed line) and walls cases at 1-mm amplitude (dot–dashed line). Due to a lack of rising Brazil nut obtained with some PBC cases with 1-mm amplitude cases, the corresponding average rise speeds were not included. We found that the number of oscillations required for the intruder to rise to the top is much greater for the 1-mm amplitude than for the 1-cm amplitude cases (about an order of magnitude greater). This was expected, as the particle displacement at each oscillation is much smaller. While there is no strong correlation of the average rise speeds with μ_r, there is a rapid increase in the rise time with μ_s for cases which exhibit the BNE. This is similar to the effect seen for the 1-cm amplitude cases.

4 DISCUSSION

4.1 Driving mechanisms

In light of the results presented in Section 3, we investigate the mechanisms which might be responsible for generating the BNE in a medium which is not confined by lateral walls. To analyse the differences in the way the BNE is driven, we consider the evolution of the height of the Brazil nut for both PBC and walls cases, for the same range of friction parameters as before ($\mu_s = 0.8$ to 1.3 in increments of 0.1 and $\mu_r = 0.2$ to 2.0 in increments of 0.2).

The evolution in time of the height of the Brazil nut (solid curve) is plotted in Fig. 9, for one set of friction parameters ($\mu_s = 0.8$ and $\mu_r = 0.4$). We compare this evolution to the changes in the standard deviation of the entire bed's height (dotted curve). This latter parameter shows oscillations driven by the periodic motion

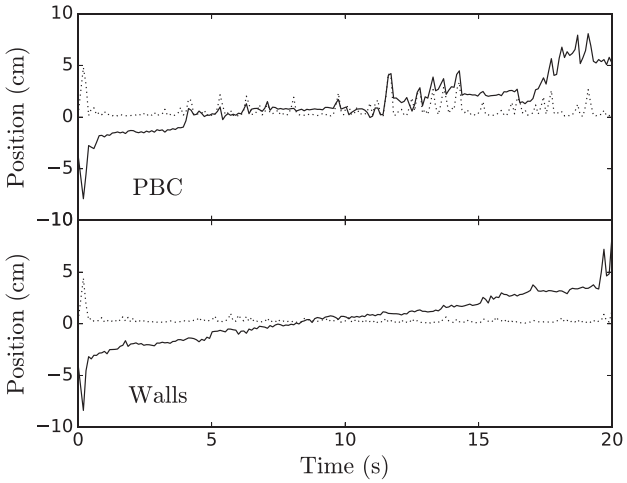

Figure 9. The height evolution of the Brazil nut (solid curve) differs for the PBC case (top) compared to the walls case (bottom). The dotted line represents the standard deviation in the height of the grains in the system. For PBC cases, the Brazil nut experiences jumps in its height, which are directly associated with the spikes in the standard deviation of grain heights. These spikes in the standard deviation represent expansions in the granular medium and the creation of voids. These two cases are for systems where the particles have friction parameters of $\mu_s = 0.8$ and $\mu_r = 0.4$.

of the bottom plate. More interestingly, large spikes in the standard deviation indicate an event where the system significantly dilates, creating void spaces in the medium. If we compare the top panel of Fig. 9 (PBC case) with the bottom panel (walls case), we can see that the BNE takes place in both cases. However, while the walls case shows a gradual increase in the height of the Brazil nut, the PBC case shows a more sporadic growth with some isolated jumps in the Brazil nut's height which are correlated with spikes in the standard deviation of the bed's height.

The difference in the evolution of the height of the Brazil nut in the two cases visible here is evident in most of the simulations. It suggests a systematic difference in the mechanism driving the BNE depending on the presence of walls, which was hinted at in the previous section (e.g. see Section 3.1). For the walls cases, the steady increase in the height of the BNE suggests that a classical convection mechanism takes place, as shown by previous authors (e.g. Knight et al. 1993). The convection mechanism is driven by particle–wall interactions which force a downward stream of particles along the walls, while interior particles are driven upwards. The size of this downward stream is limited by the size of the small grains; therefore, the Brazil nut is not able to entrain itself into the downward flow and remains at the top (see the right-hand panel of Fig. 5 for an example of this downward stream). For the PBC cases, the sporadic height evolution of the Brazil nut might suggest a possible random walk of the particle to the top. However, comparing the rise speeds of the PBC cases to the walls cases in $1g$, we find that they rise at similar speeds (see Fig. 3). This does not support the idea of a random walk, which would likely result in longer rise speeds than that found in convection-driven walls cases. Since large 'jumps' in the height of the Brazil nut are correlated with spikes in the standard deviation of the grains' height, we suggest that with PBC a void-filling mechanism (Pöschel & Herrmann 1995) drives the BNE. When a vibration lofts the material such that void space is created underneath the Brazil nut, the surrounding particles have a larger probability of filling the void space than the Brazil nut due to their smaller size. This geometric effect is able to drive the BNE, as subsequent vibration-driven lofting events further cause small particles to lodge themselves underneath the Brazil nut. In order to show that this mechanism is indeed responsible for causing the BNE in PBC cases, we analyse the standard deviation of the grains height for all simulations.

For each simulation where a full BNE cycle occurs (a Brazil nut is able to move to the top and never sinks), we use a conventional peak-finding algorithm to pick out each spike in the standard deviation of the bed's height and measure the corresponding change in the height of the Brazil nut due to this void-filling event, Δz_{vf}. In each panel of Fig. 10, we show the sum of these changes in height due to void-filling events, $\Sigma\Delta z_{vf}$, normalized by the bed depth h_{total} (each panel represents a unique initialization of the granular bed). PBC cases are represented on the left of each panel and walls cases on the right. We see that the PBC cases have systematically higher values of $\Sigma\Delta z_{vf}$, indicating that the 'jumps' of the entire bed are much more significant and frequent than with walls. This supports our claim that the BNE, under Earth gravity, is mostly driven by void-filling events with PBC, while with walls this mechanism has only some slight contribution. Since the outcome of each simulation can be highly influenced by the starting conditions, we measure the Δz_{vf} in each simulation for four different initializations to show that the difference between the two cases persists regardless of initial conditions (Fig. 10 top-right, bottom-left and -right panels). The difference in the mean of $\Sigma\Delta z_{vf}$ for the two populations (represented on the plot by a light dot–dashed line) is shown in the top-right corner of each panel.

In the top panels of Fig. 11, we compare the mean of the standard deviation spikes ($\overline{\sigma}_{z,\,vf}$), normalized by the grain radius, for each simulation (one initialization). This figure shows that void-filling events in PBC cases are driven by large fluctuations in the system height which are present in PBC cases. For walls cases, these fluctuations are limited due to particle–boundary interactions, which restrain the amount of possible system dilation.

We performed the same analysis for low-gravity simulations (amplitude of 1 cm and frequency of 0.939 rad s^{-1}), in order to assess whether or not the void-filling mechanism is also responsible for the BNE effect in PBC cases at low gravity. The ratio $\overline{\sigma}_{z,vf}$ over grain radius obtained under these conditions for one suite of simulations is shown in the bottom panels of Fig. 11. We find a similar clustering of standard deviation spikes at high values in the PBC cases compared to the Wall cases, which supports the idea that void-filling remains, under low gravity, the principal mechanism driving the BNE when PBC are used.

The lower incidence of BNE in PBC cases at low gravity and low friction values (16 per cent of the cases showed a Brazil nut incapable of rising) might be due to an attenuation in the efficiency of the void-filling mechanism compared to convection. We speculate that this might come about from a diminution of the energy transmitted to the granular bed by the bottom plate. In fact, as we keep the same value of Γ and the same amplitude as in the $1g$ simulations for the low-gravity ones, we introduce a factor of 10^{-4} in the kinetic energy transmitted to the grains compared to the $1g$ cases. With an energy four orders of magnitude lower than the one involved in Earth gravity, we can expect smaller dilation spikes, thus smaller voids created under the intruder at low friction values, and lower efficiency of the void-filling process compared to $1g$. However, Fig. 11 shows that the mechanism is still active in low gravity.

The void-filling mechanism has been previously studied with PBC by Schröter et al. (2006). The authors showed that a system

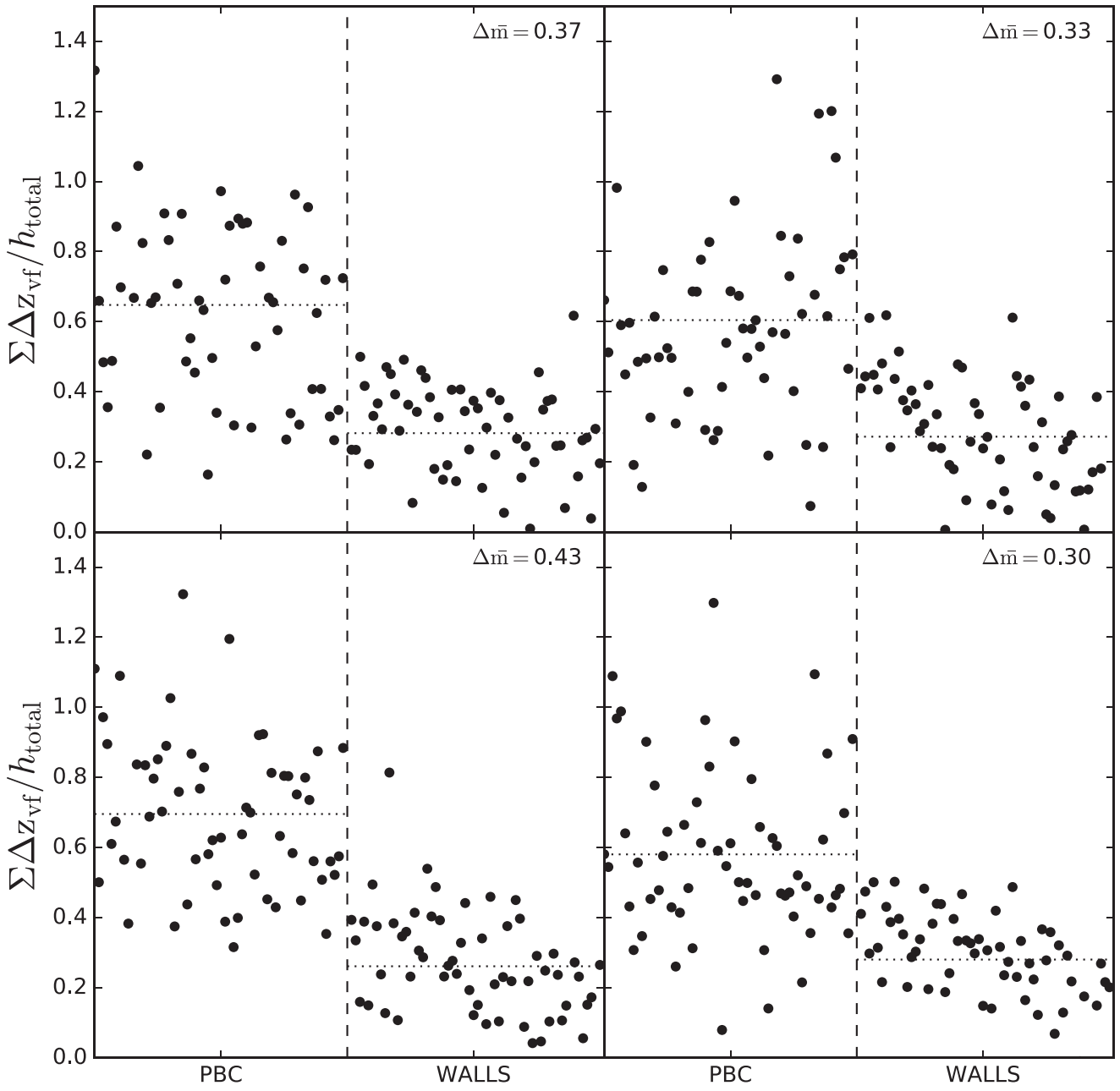

Figure 10. Sum of the changes in Brazil nut height due to void-filling events for four different initializations of the granular bed. Each point represents a single simulation. Each simulation results in a BNE (the intruder rises to the top of the granular system). For each simulation, the change in the intruder height due to a void-creating event is tracked. The thick vertical dashed lines separate simulations with PBC and simulations with wall boundaries. The dot–dashed lines represent these mean values of $\Sigma\Delta z_{vf}$ for each boundary condition, and $\Delta\bar{m}$ is the difference in the mean values. The values here represent the total net change in the intruder height over the course of the entire simulation. Points for PBC cases cluster at high values, while points for walls cases cluster at low values. Evidently, two different mechanisms drive the BNE for these two different setups.

bounded by walls can have a BNE driven by convection, while a PBC case is likely driven by void-filling events. However, these authors speculated that the vibrations which induce void-filling events are much smaller than those which drive convection. Here, we show that for the same vibrational energy, two different mechanisms arise due to differences in the boundary conditions.

This paper marks the first attempt at showing that a void-filling mechanism may be responsible for size-segregation of large grains on an asteroid. By using boundary and gravity conditions which more closely resemble an asteroid environment, we suggest that vibrations are able to drive a boulder to the surface of an asteroid. Furthermore, the void-filling mechanism is also enhanced by a larger size ratio between particles, and, unlike the convection mechanism seen with walls, it does not depend on the bed depth (Schröter et al. 2006)). Previous studies (e.g. Taguchi 1992) have shown that convection-driven mechanisms are limited to the upper 10 or so grain heights of a system. After a certain depth, convection can no longer efficiently drive BNE. Since the void-filling mechanism occurs independently of bed depth, a boulder entrained deep below the surface may still be able to segregate upwards. Finally, the void-filling mechanism is characterized by independent lofting events and does not necessarily require a continuity in the seismic

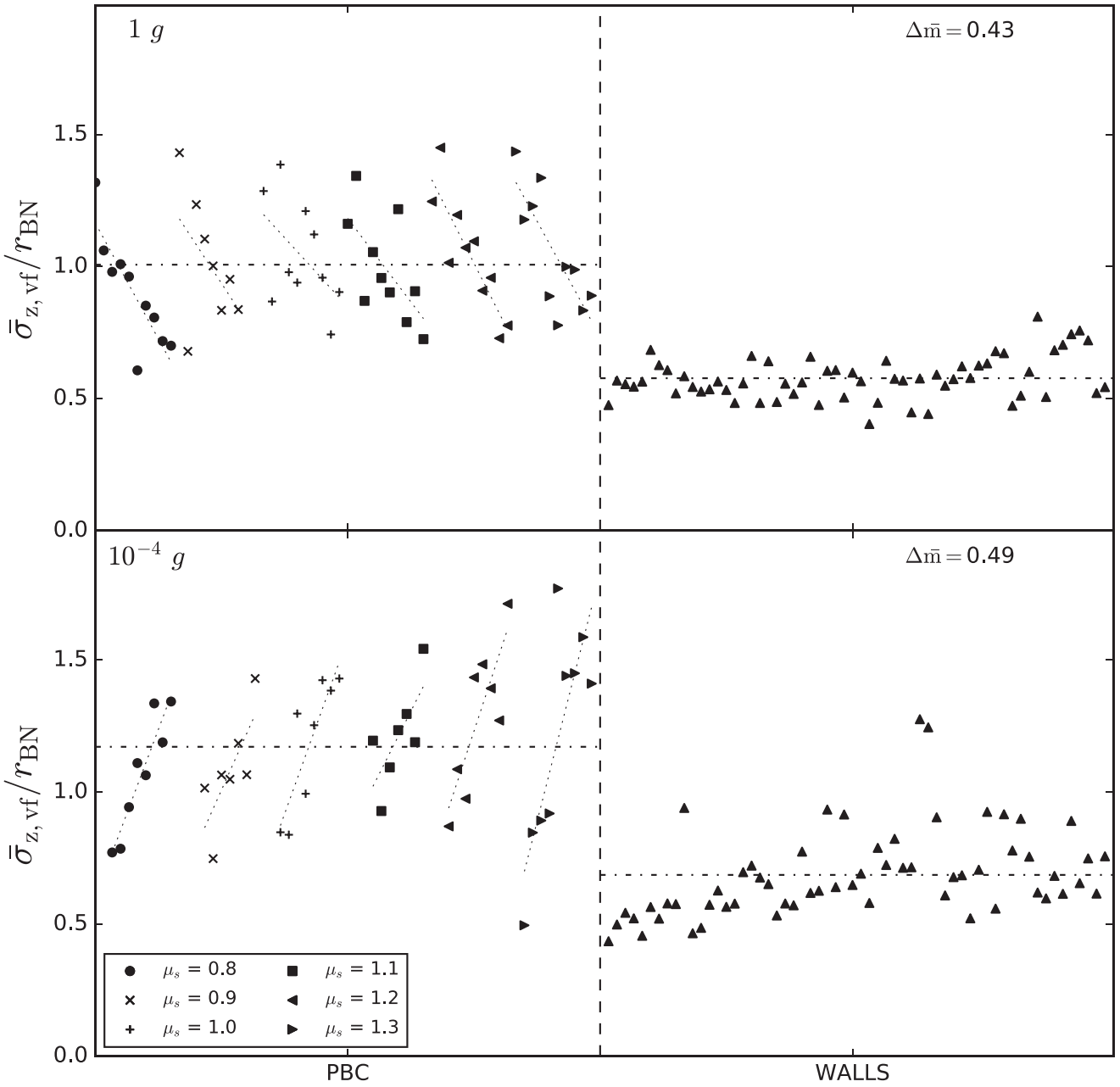

Figure 11. Mean of the grain height standard deviation during void-filling events. The thick vertical dashed lines separate simulations with PBC and simulations with wall boundaries. The horizontal dot–dashed lines represent the mean values of $\overline{\sigma}_{z,\mathrm{vf}}$ for each boundary condition, and $\Delta\bar{m}$ is the difference in mean values. The granular systems in these two setups behave differently in response to the periodic forcing. For PBC cases, the grains are more free to dilate and create voids. For walls cases, the walls inhibit the grains from expanding too much. Hence, the standard deviation in the height of the grains is systematically larger for PBC cases than it is for walls cases. We plot the PBC cases with unique scatter points based on the static friction value, μ_s, used in each simulation. Simulations with μ_s of 0.8, 0.9, 1.0, 1.1, 1.2 and 1.3 are represented by circles, x-marks, crosses, squares, left-facing triangles, and right-facing triangles, respectively. Each of the six groups of μ_s values are sorted in order of increasing rolling friction, μ_r. The dotted lines for each μ_s group represent regression lines establishing the dependence of $\overline{\sigma}_{z,\mathrm{vf}}$ with μ_r for each unique μ_s.

shaking. Thus it can be driven by independent shocks undergone by an asteroid over its lifetime. All of these facts make the void-filling mechanism particularly relevant to the asteroid environment.

4.2 Interplay between gravity and rolling friction

Unlike previous studies, we have attempted to clarify the influence of material property on the rise speed of the Brazil nut for different boundary conditions and different gravity regimes. As Section 3.3 shows, a low-gravity system changes the dynamical effects of rolling friction. In Earth gravity, PBC cases showed a negative correlation with μ_r; meanwhile, a positive correlation was found in low gravity. Furthermore, an inspection of Fig. 6 shows that at intermediate gravity, 10^{-2} g, there seems to be no correlation with μ_r at all. These clues hint at a variation in the granular flow of this system across different gravity regimes.

The PBC simulations in Fig. 11 are uniquely identified based on the static friction coefficient of the grains. In each panel, grains are

grouped by increasing values of μ_s (from left to right), and each of these μ_s groupings are sorted in order of increasing μ_r (again from left to right), when the data are available. We plotted, for each μ_s group, the regression line which best fits the dependence of $\overline{\sigma}_{z,vf}$ with μ_r for that particular group. We find that for Earth-gravity conditions, $\overline{\sigma}_{z,vf}$ clearly decreases with μ_r for every value of μ_s. At $10^{-4}g$, the trend reverses, and $\overline{\sigma}_{z,vf}$ increases with μ_r for every value of μ_s.

These trends suggest that, in Earth-gravity conditions, rolling friction diminishes dilation events in the system. Grains have a more difficult time flowing past one another as the system locks up. Even if voids are created, the grains are incapable of flowing into these voids. In low gravity, rolling friction enhances the strength of dilation events in the system. The larger average value of $\overline{\sigma}_{z,vf}$ (dot–dashed horizontal lines in Fig. 11) for PBC cases suggests that the system is lofted higher and for a longer time in a lower gravity environment. Systems with high-friction grains will be able to create larger void spaces, as the system is able to dilate due to stronger contact forces. This stronger force network may further feed into longer lofting times as subsequent impulses from the bottom plate are more efficiently transmitted upwards. Thus, rather than diminishing the BNE, high rolling friction, combined with longer lofting times, may create large enough void spaces that the void-filling mechanism is enhanced. Therefore, while these rougher grains typically inhibit granular flow, they can create larger void spaces which allow grains to move more freely in low gravity.

While a full physical model of this process is beyond the scope of this study, we can begin to see its outlines. Namely, there are two important dynamical time-scales involved in this process, whose predominancy seems to reverse with gravity; namely, the first being a gravitational time-scale, and the second being a granular flow time-scale. The gravitational time-scale is well known, being simply determined by the size of the system and the local gravitational acceleration. The granular flow time-scale is more elusive to determine, as there are combined non-linearities which come into play in a granular system. However, it is clear that what will chiefly determine the efficiency of granular flow, and the possibility of BNE in a semi-boundless system, is the incidence of voids in that system.

5 CONCLUSION

We performed numerical simulations of vibration-driven grains. We attempted to advance the current understanding of size segregation among asteroid regolith grains in low gravity by performing simulations with realistic grain physical properties, boundary conditions and gravity environment. Previous studies that used simulations of the BNE in the context of asteroids ran simulations with walls. Here, we wanted to better mimic the asteroid environment by removing these lateral boundaries, which are probably not the most appropriate representation of an asteroid interior. Instead, we implemented PBC. We were able to show that for a wide range in friction properties, the BNE occurs even when PBC are used. We also explored a broad range of friction levels, from medium to high, which led us to the conclusion that a different mechanism drives the BNE in walls compared with PBC cases. While granular convection is well known to drive the BNE with walls, we have shown that a void-filling mechanism is actually predominant when PBC are turned on. The void-filling mechanism occurs when a vibration causes the granular system to dilate, creating void spaces in the medium. In Earth gravity, a sufficiently fluid granular system allows the creation of void spaces which affords an opportunity for large-scale displacement of particles. Due to the size difference between the large intruder and the surrounding grains, the smaller grains have a higher probability of filling the void space created below the intruder. This allows the BNE to occur in a system without confining wall boundaries, which are required for granular convection to occur.

For a better representation of the asteroid environment, we also studied the BNE in low gravity ($10^{-4}g$). We found that both convection for walls cases and the void-filling mechanism for PBC cases are still able to occur, however with striking differences compared to the $1g$ simulations. For walls cases, we found that convection is counterintuitively enhanced for higher friction and speculate that the lower packing in low-gravity cases may be responsible for this behaviour. For PBC cases, we found that the void-filling mechanism is still able to occur, and that the total number of forcing cycles in the lower gravity environment is comparable to that in Earth gravity. However, our exploration of a broad range of rolling friction levels highlighted major differences in the effect of this rolling friction on the BNE. Unlike for the $1g$ cases, where a higher rolling friction freezes the void-filling mechanism (the grains are no longer able to fill the voids), low-gravity cases show a reverse trend, where a higher rolling friction level actually enhances the BNE. We suggest that this difference comes from a change in the predominant time-scale for the system. In $1g$, the gravity does not allow long lofting time, and therefore, the higher the rolling friction, the greater the inhibition of the grains' reorganization, which occurs on a different time-scale, the granular flow time-scale. Conversely, in low gravity, the granular flow time-scale becomes more important as the gravity allows much longer lofting time, enabling frictional particles to fill the voids anyway. In addition, a higher rolling friction results in the creation of more voids to be filled by the particles, which results in the inversion of the trend of the rise speed with μ_r for Earth- and low-gravity cases. We propose that the transition between the predominancy of one regime or another may occur around $10^{-2}g$, as the influence of μ_r on the rise speed is for this case almost non-existent.

Finally, we also studied small-amplitude vibrations, where the amplitude is much smaller than the size of the grains. We found that the BNE is less likely to occur. This is especially true for cases with PBC. The PBC cases require sufficiently large void spaces to be created during the vibration in order to drive the BNE. If the shaking amplitude is much smaller than a grain size, then the subsequent voids are likely to be small as well. Hence, the grains are unable to fill in voids created underneath the intruder. Despite this, we find that a few PBC cases are able to exhibit the BNE. These are cases where both the static and rolling friction are high. It is possible that in these cases the friction between grains is sufficient to allow voids to slowly grow between subsequent shakes until they become large enough for a small particle to occupy them. Furthermore, a real asteroid will have grains which span a wider size distribution. It is possible that grains with a size smaller than the oscillation amplitude might be able to self-segregate efficiently, influencing the segregation process at larger scales.

The void-filling mechanism is a promising mechanism to explain features on actual asteroids. Images and radar observations collected during space missions indicate the presence of boulders at the surface of asteroids. In fact, a boulder is the target of the Asteroid Retrieval Mission (ARM) under study at NASA, which aims at collecting a boulder from the surface of the asteroid 2008 EV5 and placing it on a cis-lunar orbit for later rendezvous by astronauts sent to interact with it (Abell et al. 2015). The physical properties of boulders present on asteroid surfaces are intimately related to their origin and history. Determining the mechanism bringing them to the surface (BNE or any other mechanism) can provide valuable clues

to determine their physical properties. Future work could build on the simulations performed in the present study and explore a larger parameter space, always with the aim of characterizing asteroid interiors and environments more realistically.

ACKNOWLEDGEMENTS

Simulations were performed on the YORP cluster administered by the Center for Theory and Computation, part of the Department of Astronomy at the University of Maryland, and the Deepthought2 HPC cluster at the University of Maryland. This material is based in part on work supported by the US National Aeronautics and Space Administration under Grant nos. NNX14AO36G and NNX15AH90G issued through the Office of Space Science. PM acknowledges support by the French Space Agency CNES and the European Space Agency.

REFERENCES

Abell P. A., Barbee B. W., Chodas P. W., Kawaguchi J., Landis R. R., Mazanek D. D., Michel P., 2015, in Michel P., DeMeo F. E., Bottke W. F., eds, Asteroids IV. Univ. Arizona Press, Tucson, p. 855
Asphaug E., 2007, LPI Contrib., 1338, 2432
Asphaug E., King P. J., Swift M. R., Merrifield M. R., 2001, LPI Contrib., 1080, 1708
Barabási A.-L., Albert R., Hirata N., Schiffer P., 1999, Physica A, 266, 366
Barnouin-Jha O. S. et al., 2008, Icarus, 198, 108
Bottke W. F., Durda D. D., Nesvorný D., Jedicke R., Morbidelli A., Vokrouhlický D., Levison H. F., 2005, Icarus, 179, 63
Bottke W. F., Brož M., O'Brien D. P., Campo Bagatin A., Morbidelli A., Marchi S., 2015, in Michel P., DeMeo F. E., Bottke W. F., eds, Asteroids IV. Univ. Arizona Press, Tucson, p. 701
Cheng A. F., Izenberg N., Chapman C. R., Zuber M. T., 2002, Meteorit. Planet. Sci., 37, 1095
Chesley S. R. et al., 2003, Science, 302, 1739
Delbo' M., dell'Oro A., Harris A. W., Mottola S., Mueller M., 2007, Icarus, 190, 236
Delbo' M., Mueller M., Emery J. P., Rozitis B., Capria M. T., 2015, in Michel P., DeMeo F. E., Bottke W. F., eds, Asteroids IV. Univ. Arizona Press, Tucson, p. 107
Delbo M. et al., 2014, Nature, 508, 233
Fujiwara A. et al., 2006, Science, 312, 1330
Garcia R. F., Murdoch N., Mimoun D., 2015, Icarus, 253, 159
Gray J., Thornton A., 2005, Proc. R. Soc. A 461, 1447
Güttler C., von Borstel I., Schräpler R., Blum J., 2013, Phys. Rev. E, 87, 044201
Knight J. B., Jaeger H. M., Nagel S. R., 1993, Phys. Rev. Lett., 70, 3728
Kudrolli A., 2004, Rep. Prog. Phys., 67, 209
Matsumura S., Richardson D. C., Michel P., Schwartz S. R., Ballouz R.-L., 2014, MNRAS, 443, 3368
Merline W. J., Chapman C. R., 2001, Meteorit. Planet. Sci. Suppl., 36, A132
Michel P., Richardson D. C., 2013, A&A, 554, L1
Michel P., Benz W., Tanga P., Richardson D. C., 2001, Science, 294, 1696
Michel P., O'Brien D. P., Abe S., Hirata N., 2009, Icarus, 200, 503
Michel P., Richardson D. C., Durda D. D., Jutzi M., Asphaug E., 2015, in Michel P., DeMeo F. E., Bottke W. F., eds, Asteroids IV. Univ. Arizona Press, Tucson, p. 341
Michikami T. et al., 2008, Earth, Planets, Space, 60, 13
Miyamoto H. et al., 2007, Science, 316, 1011
Murdoch N., Rozitis B., Green S. F., Michel P., de Lophem T.-L., Losert W., 2013, MNRAS, 433, 506
Murdoch N., Sánchez P., Schwartz S. R., Miyamoto H., 2015, in Michel P., DeMeo F. E., Bottke W. F., eds, Asteroids IV. Univ. Arizona Press, Tucson, p. 767
Orlova N. S., 1962, in Kopal Z., Mikhailov Z. K., eds, Proc. IAU Symp. 14, The Moon. Academic Press, New York, p. 411
Perera V., Jackson A. P., Asphaug E., Ballouz R.-L., 2016, Icarus, 278, 194
Pöschel T., Herrmann H. J., 1995, Europhys. Lett., 29, 123
Richardson D. C., Quinn T., Stadel J., Lake G., 2000, Icarus, 143, 45
Richardson D. C., Leinhardt Z. M., Melosh H. J., Bottke W. F., Jr, Asphaug E., 2002, in Bottke W. F., Jr, Cellino A., Paolicchi P., Binzel R. P., eds, Asteroids III. Univ. Arizona Press, Tucson, p. 501
Richardson J. E., Melosh H. J., Greenberg R., 2004, Science, 306, 1526
Richardson D. C., Michel P., Walsh K. J., Flynn K. W., 2009, Planet. Space Sci., 57, 183
Richardson D. C., Walsh K. J., Murdoch N., Michel P., 2011, Icarus, 212, 427
Richardson D. C., Blum J., Weinhart T., Schwartz S. R., Michel P., Walsh K. J., 2012, AAS/Division for Planetary Sciences Meeting Abstracts, 105.06
Rosato A., Standburg K., Prinz F., Swendsen R., 1987, Phys. Rev. Lett., 1038, L58
Schröter M., Ulrich S., Kreft J., Swift J. B., Swinney H. L., 2006, Phys. Rev. E, 74, 011307
Schwartz S., Richardson D., Michel P., 2012, Granul. Matter, 14, 363
Stadel J. G., 2001, PhD thesis, Univ. Washington
Taguchi Y.-h., 1992, Phys. Rev. Lett., 69, 1367
Tancredi G., Maciel A., Heredia L., Richeri P., Nesmachnow S., 2012, MNRAS, 420, 3368
Yeomans D. K., Konopliv A. S., Barriot J.-P., 1997, J. Geophys. Res., 102, 23775
Yoshikawa M., Kawaguchi J., Fujiwara A., Tsuchiyama A., 2015, in Michel P., DeMeo F. E., Bottke W. F., eds, Asteroids IV. Univ. Arizona Press, Tucson, p. 397
Yu Y., Richardson D. C., Michel P., Schwartz S. R., Ballouz R.-L., 2014, Icarus, 242, 82
Zhang Y., Richardson D. C., Barnouin O. S., Maurel C., Michel P., Schwartz S. R., Ballouz R.-L., Li J., 2016, Icarus, in press

This paper has been typeset from a TEX/LATEX file prepared by the author.